



HAL
open science

Different Methods in Assessing El Niño Flavors Lead to Opposite Results

Isma Abdelkader Di Carlo, Pascale Braconnot, Matthieu Carré, Mary Elliot,
Olivier Marti

► **To cite this version:**

Isma Abdelkader Di Carlo, Pascale Braconnot, Matthieu Carré, Mary Elliot, Olivier Marti. Different Methods in Assessing El Niño Flavors Lead to Opposite Results. *Geophysical Research Letters*, 2023, 50 (15), 10.1029/2023gl104558 . hal-04184718

HAL Id: hal-04184718

<https://hal.science/hal-04184718>

Submitted on 22 Aug 2023

HAL is a multi-disciplinary open access archive for the deposit and dissemination of scientific research documents, whether they are published or not. The documents may come from teaching and research institutions in France or abroad, or from public or private research centers.

L'archive ouverte pluridisciplinaire **HAL**, est destinée au dépôt et à la diffusion de documents scientifiques de niveau recherche, publiés ou non, émanant des établissements d'enseignement et de recherche français ou étrangers, des laboratoires publics ou privés.





Geophysical Research Letters®



RESEARCH LETTER

10.1029/2023GL104558

Different Methods in Assessing El Niño Flavors Lead to Opposite Results

Isma Abdelkader Di Carlo¹ , Pascale Braconnot¹ , Matthieu Carré^{2,3} , Mary Elliot⁴, and Olivier Marti¹ 

¹IPSL/Laboratoire des Sciences du Climat et de l'Environnement, unité mixte CEA-CNRS-UVSQ, Université Paris Saclay, Gif-sur-Yvette, France, ²IPSL/Laboratoire d'Océanographie et du Climat: Expérimentations et Approches Numériques (CNRS-IRD-MNHN-Sorbonne Universités), Paris, France, ³Facultad de Ciencias y Filosofía, LID, CIDIS, Universidad Peruana Cayetano Heredia, Lima, Peru, ⁴LPG (Laboratoire de Planétologie et Géosciences), UMR, Nantes Université, France, France

Key Points:

- Two equivalent indicators of El Niño-Southern Oscillation (ENSO) flavors in the present give opposite evolution during the Holocene
- Results show that the conflict between methods comes from the representation of ENSO flavor patterns on short and long timescales
- A proper assessment must account for the indicator's patterns and calibration, as well as the climate mean-state change over time

Supporting Information:

Supporting Information may be found in the online version of this article.

Correspondence to:

I. Abdelkader Di Carlo,
isma.abdelkaderdicarlo@lscce.ipsl.fr

Citation:

Abdelkader Di Carlo, I., Braconnot, P., Carré, M., Elliot, M., & Marti, O. (2023). Different methods in assessing El Niño flavors lead to opposite results. *Geophysical Research Letters*, 50, e2023GL104558. <https://doi.org/10.1029/2023GL104558>

Received 16 MAY 2023

Accepted 28 JUN 2023

Abstract El Niño-Southern Oscillation (ENSO) flavors have been defined to characterize ENSO events and their teleconnections. Studying El Niño flavor evolution during the Holocene period can provide valuable insights into changes over long time scales. We investigated ENSO flavor evolution using simulations spanning the last 6,000 years and present-day observations. Two approaches to computing ENSO flavors, in agreement in the present, lead to opposite trends in the last 6,000 years. The methods also differ significantly in their representation of ENSO flavor patterns. However, incorporating the sensitivity of the methods to calibration periods and mean state changes yields similar interpretations of ENSO variability changes. Both methods suggest an increase in El Niño variability spreading to the west and east tropical Pacific over the past 6,000 years. Standardizing El Niño flavor definitions is necessary for meaningful comparisons between studies and robust climate variability analysis.

Plain Language Summary El Niño events are the dominant mode of interannual variability. Looking at El Niño events in the past, during the Holocene period, could shed light on the linkages between the characteristics of El Niño patterns and changes in the climate mean state. Different indicators are used to characterize El Niño pattern diversity depending on the available data. While equivalent under present-day conditions, these indicators lead to opposite conclusions on the evolution of El Niño patterns over the last 6,000 years. An in-depth analysis indicates that all the methods suggest that El Niño-related variance has spread to the west and east tropical Pacific over time when accounting for sensitivity to calibration periods and changes in the mean state during the Holocene. Agreeing on a standard definition for El Niño flavors is essential for accurate comparison between studies and for avoiding misleading conclusions.

1. Introduction

The tropical Pacific Ocean is the center of action of the El Niño-Southern Oscillation (ENSO), the dominant mode of tropical climate variability (Philander, 1990; Vecchi & Wittenberg, 2010). This phenomenon changes temperature and weather patterns via atmospheric teleconnections, thus affecting ecosystems and human societies worldwide (Cai et al., 2021; Collins et al., 2010). However, El Niño's response to global warming is still unclear in model projections and limits future predictions (Cai et al., 2014, 2021; Callahan et al., 2021; DiNezio et al., 2012; Fredriksen et al., 2020; Freund et al., 2020; Wengel et al., 2021).

Additional complexity arises from the diversity of El Niño events, or flavors, which is now well characterized (Capotondi et al., 2015; Timmermann et al., 2018). There is no robust consensus regarding the changes in El Niño events' diversity under climate change (Lee & McPhaden, 2010; McPhaden et al., 2011; Yeh et al., 2009). For example, models that predict an El Niño-like warming in the future have been associated with an increase in Eastern Pacific (EP) El Niño events (Fredriksen et al., 2020), or with more Central Pacific (CP) and fewer EP events (Freund et al., 2020).

The Holocene period, which began 10,000 years ago, provides a long-time-scale perspective on the links between changes in the mean state and El Niño variability, primarily related to orbitally driven changes in insolation. Throughout the Holocene, the seasonal cycle of incoming solar radiation at the top of the atmosphere decreases in the Northern Hemisphere and increases in the Southern Hemisphere due to slow changes in the Earth's orbital

© 2023. The Authors.

This is an open access article under the terms of the [Creative Commons Attribution License](https://creativecommons.org/licenses/by/4.0/), which permits use, distribution and reproduction in any medium, provided the original work is properly cited.

parameters (Braconnot et al., 2019). Models and marine data show a reduction of ENSO variability in the mid-Holocene compared with the present (Brown et al., 2020; Carré et al., 2014, 2021; Emile-Geay et al., 2016). The last 6,000 years allow us to explore whether the diversity of El Niño events may change with the climate mean state.

A limited amount of studies tried to characterize the changes in El Niño flavors from paleoclimate simulations (e.g., Luan et al., 2012; Karamperidou et al., 2015) and even less from paleoclimate data. One of the first attempts to detect past changes in ENSO flavors in paleoclimate records during the Holocene was based on fossil bivalve records from Peru (Carré et al., 2014). This study showed a period of negatively skewed anomalies about 7,000 years ago and it was interpreted as a period dominated by CP El Niño events. Recently, Holocene changes in ENSO flavors were explored using the ratio of interannual variability changes recorded in the EP and CP regions, using boxes corresponding to the location of the fossil coral and bivalve records (Carré et al., 2021). The variance ratio between the EP and CP boxes in four transient simulations had either decreased or barely changed from 6,000 years ago to the present, which is qualitatively consistent with proxy observations (Carré et al., 2021). This is opposite to Karamperidou et al. (2015)'s results. Using two snapshot simulations of a mid-Holocene climate and pre-industrial conditions, they computed the variance of EP and CP El Niño events as defined by Takahashi et al. (2011) and found an increase in the variance of EP El Niño events and no changes in CP El Niño events in the preindustrial run compared with the mid-Holocene.

Here, we compare results obtained with the two types of methods using transient simulations of the last 6,000 years with two reference versions of the IPSL model (Braconnot et al., 2019), as well as two historical datasets (Hirahara et al., 2014; Huang et al., 2017). We analyze the reasons for the difference between the results of Carré et al. (2021) and Karamperidou et al. (2015). We do not judge which definition of ENSO flavors is best and note that the choice of methods should depend on the analysis context. We, therefore, question the way of interpreting the indicators and the exact meaning of the indicators themselves. We also discuss the implication for model-data comparisons and for assessing ENSO flavor changes in a context of mean state shift that might alter ENSO patterns.

Section 2 describes the historical datasets and transient simulations, the two methods of El Niño flavors' computation, and the multi-linear regression approach chosen to characterize El Niño pattern shifts. Section 3 presents the different approaches to El Niño flavor shifts over the Holocene and present times, and discusses how to interpret the results of the two methods.

2. Methods

2.1. Transient Holocene Simulations and SST Observation Data

The two transient simulations used in this study, V1r01 and Sr02, are described in Braconnot et al. (2019) and were also part of the model-data comparison in Carré et al. (2021). The IPSL fully coupled model includes the energy, water, and carbon cycle between the atmosphere, ocean, land, and ice. For V1r01, obtained with the IPSL-CM5 model, the atmosphere has a horizontal resolution of 96 points in longitude and latitude and a vertical resolution of 39 levels. The ocean has a resolution of 182 points in longitude, 149 points in latitude, and 31 vertical levels. The model version is described in Dufresne et al. (2013). Sr02 is run with a modified model version with a different soil hydrological scheme over land and a dynamical vegetation module (Braconnot et al., 2019). It also has a higher horizontal atmospheric resolution of 144 points in longitude and 143 in latitude. Both simulations are run from 6,000 BP to 0 BP (1950 CE). The initial state corresponds to a mid-Holocene simulation with the corresponding model version. Earth orbital parameters and trace gases are updated annually (Braconnot et al., 2019), following the experimental protocol proposed by Otto-Bliesner et al. (2017).

In both versions of the IPSL model, the equatorial upwelling extends too far west, eroding the warm pool, and there is a tendency to produce too many spring El Niño events (Dufresne et al., 2013; Saint-Lu et al., 2016). Dynamic and thermodynamic feedbacks are smaller than observed, and ENSO variability is underestimated (Bellenger et al., 2014).

To compare the model results with observations, we use two historical SST datasets: COBE-SST2 (Hirahara et al., 2014) and ERSSTv5 (Huang et al., 2017). The temporal coverage of COBE-SST2 extends from 1850 to 2019 and ERSSTv5 from 1854 to 2023. ERSSTv5 is derived from the International Comprehensive Ocean-Atmosphere

Dataset (ICOADS). The SST field from COBE-SST2 is reconstructed from in-situ SST and sea ice concentration observations. The common time frame for comparing the SST datasets and simulations is 1854–1950 CE. To have the same comparison framework, COBE-SST2, ERSSTv5, V1r01, and Sr02 were remapped to a resolution of 1° in both latitude and longitude.

2.2. Estimation of El Niño Flavors

Most definitions of ENSO diversity in the present, future, or past climates fall into two categories. In the first one, an Empirical Orthogonal Functions (EOF) approach is preferred to retrieve specific ENSO patterns (e.g., Takahashi et al., 2011; Kao and Yu, 2009; Ashok et al., 2007). Here, we use the indicator provided by Takahashi et al. (2011). We call it M1, and the way to estimate the EP and CP El Niño flavors is by rotating the first two principal components, PC1 and PC2, of SST anomalies in the tropical Pacific Ocean (10°S–10°N, 110°E–60°W):

$$E_1 = \frac{PC1 - PC2}{\sqrt{2}} \quad (1)$$

$$C_1 = \frac{PC1 + PC2}{\sqrt{2}} \quad (2)$$

The E_1 flavor emphasizes a type of El Niño that is more extreme with maximum anomaly located in the eastern tropical Pacific. The C_1 flavor defines less extreme El Niño events in the central equatorial Pacific and some La Niña events. The E_1 and C_1 axes are orthogonal and, according to Takahashi et al. (2011), have dynamical meaning because they characterize anomalies related to changes in large-scale ENSO dynamics.

In the second category, ENSO flavor indicators are estimated from the evolution of spatially averaged SST over specific areas (boxes) in the tropical Pacific that best represent EP and CP El Niño events (e.g., Kug et al. (2009); Yeh et al. (2009); Ren and Jin (2011)). E_1 and C_1 flavors, as computed above, correlate well with SSTs in the Niño4 (5°S–5°N, 160°E–150°W) and Niño1+2 (10°S–0°, 90°W–80°W) boxes. Based on the M1 method (Equations 1 and 2), Takahashi et al. (2011) proposed a way to approximate E_1 and C_1 through the linear combination of the SST anomalies in the Niño4 and Niño1+2 boxes. This method is called M2 and chosen to generically represent methods that compute ENSO flavors through the use of Niño boxes or boxes related to proxy records (e.g., Ren and Jin, 2011; Carré et al., 2021). Here, we use the same definition as Takahashi et al. (2011):

$$E_2 = Niño_{1+2} - 0.5 \times Niño_4 \quad (3)$$

$$C_2 = 1.7 \times Niño_4 - 0.1 \times Niño_{1+2} \quad (4)$$

With this definition, M1 and M2 provide similar results for the recent climatic period (Figure S1 in Supporting Information S1). For M2 and M1, E and C flavors, are estimated using the interannual band of SST anomalies, obtained first by detrending SSTs and then applying a 2–7 year bandpass filter. The principal components computed in M1, PC1 and PC2, were standardized to unit standard deviation. For both methods, we take the October–April averages of the computed E and C flavors, that are then standardized to unit standard deviation. We note that, for M1, the EOF analysis gives both the patterns and time series of E_1 and C_1 , while M2 is empirically computed, and thus we only have access to the time series of E_2 and C_2 . We regress the times series onto the SST anomaly field to have the associated patterns. To stay consistent, we use the same method for E_1 and C_1 . The regressed E_1 and C_1 give the same results as their original EOF projections.

To reflect changes in the relative contribution of E and C flavors in total ENSO variability, we compute estimates of the ratios of E over C, expressed as variance ratios for both methods. To show the long-term evolution of the ratio, we use a rolling window of 500 years over the Holocene. We also employ a window of 10 years to show the variability of ENSO flavors and agreement between methods in present times. We note that the shorter 10-year window and observational period are not long enough to capture long-term changes in ENSO variability, which requires at least 250 years (Stevenson et al., 2013; Wittenberg, 2009).

2.3. Multi-Linear Regression

To interpret the differences between the two methods, we analyze how the E and C flavors represent the time series variability in the Niño1+2 and Niño4 boxes, the regions at the eastern and western ends of ENSO activity.

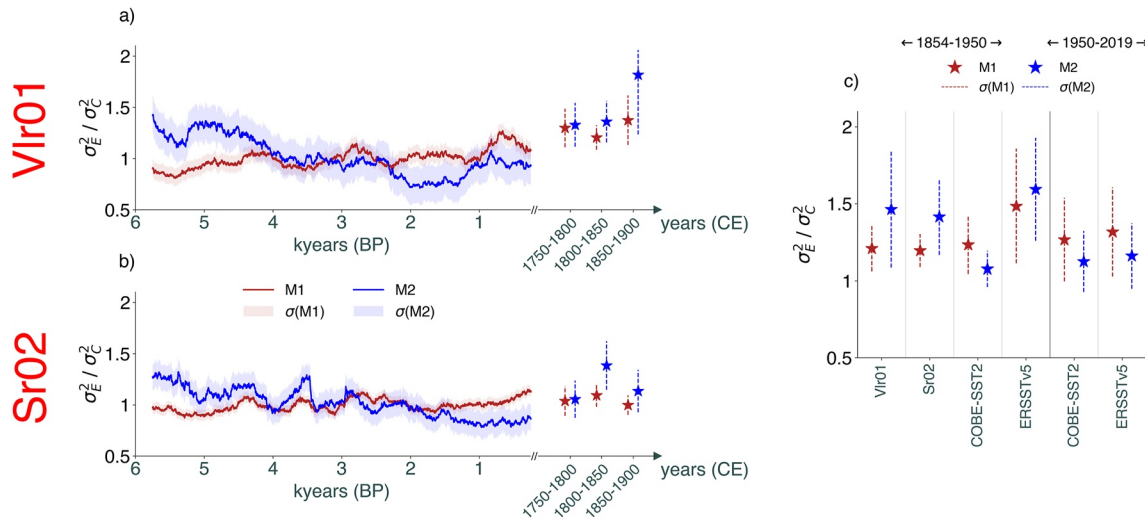


Figure 1. Evolution of the variance ratios of the E over C flavors during the Holocene for the simulations (a) Vlr01 and (b) Sr02, and for (c) present times. In (a) and (b), the solid lines represent E's 500-year rolling variance ratio over C (red for M1 and blue for M2). The shadings represent an error bar estimated from the variance ratio using a bootstrap approach with 1000 random 500-year non-overlapping windows. The x-axis represents the time in kyears BP (from left to right). In (c), we represented the mean of the 10-year rolling variance ratios of E over C, for each simulation (Vlr01, Sr02) and observational datasets (ERSSTv5, COBE-SST2), as a scatter plot. The dashed lines represent the 95% confidence interval of the mean, evaluated by bootstrap (10,000 repetitions). The scatter plots in (a) and (b) are also evaluated similarly for 1750–1800, 1800–1850, and 1850–1900 CE for both simulations. Each 50-year block comes from a separate analysis where we computed M1 and M2 in non-overlapping successive 50-year windows.

We first compute the average SST anomaly time series over each box. The variance is decomposed as the linear combination of the E and C flavors' variance:

$$\sigma_{Ni\tilde{n}o_y}^2 = \alpha \times \sigma_{E_i}^2 + \beta \times \sigma_{C_i}^2 + \gamma \quad (5)$$

where $i = 1$ or $i = 2$, $\sigma_{Ni\tilde{n}o_y}^2$ is the variance of $Ni\tilde{n}o_y = Ni\tilde{n}o_{1+2}$ or $Ni\tilde{n}o_4$, σ_E^2 is the variance of the E flavor with method M_i , and σ_C^2 is the variance of the C flavor estimated by method M_i . Variances were calculated over a window of 500 years, sliding over the 6,000–0 BP period. The regression coefficients are α and β , and γ is the residual. We computed these coefficients using a lasso regression model because it avoids overfitting by adding a penalty term to too-large coefficients (Tibshirani, 1996).

3. Different Approaches of El Niño Flavor Changes

3.1. Relative Changes Over the Last 6,000 Years

A surprising first result emerges from comparing the relative evolution of the E and C flavor variance ratios in the two transient simulations (Figures 1a and 1b). The ratio increases for both simulations when computed with M1 and decreases when calculated using M2. The two methods lead to opposite conclusions on the relative evolution of ENSO throughout the Holocene when they should provide similar results. We hypothesize that the differences between Carré et al. (2021) and Karamperidou et al. (2015) come from the methods themselves.

Therefore, the difference between M1 and M2 might reflect specific Holocene variability or result from some of the model biases listed above. We first investigate the robustness of M2 and M1 estimates in the recent period from observations.

Although estimations of the E and C flavors for COBE-SST2 and ERSSTv5 match almost perfectly for the period 1950 to 2019 (Figure 1c and Figure S1 in Supporting Information S1), differences also emerge. Indeed, from 1854 to 1950, the agreement between the two datasets is not as good (Figure 1c). This can be attributed to the time window (1950–2010) used in Takahashi et al. (2011) to calibrate M2 from M1, which is too short to document the range of El Niño event diversity properly (Equations 3 and 4). A calibration for the 1854–1950 period would yield $E_2 = -1.63 \times Ni\tilde{n}o_4 + 2.86 \times Ni\tilde{n}o_{1+2}$ and $C_2 = 4.28 \times Ni\tilde{n}o_4 - 1.73 \times Ni\tilde{n}o_{1+2}$ for COBE-SST2, and $E_2 = -0.34 \times Ni\tilde{n}o_4 + 1.58 \times Ni\tilde{n}o_{1+2}$ and $C_2 = 2.66 \times Ni\tilde{n}o_4 - 0.81 \times Ni\tilde{n}o_{1+2}$ for ERSSTv5. Differences

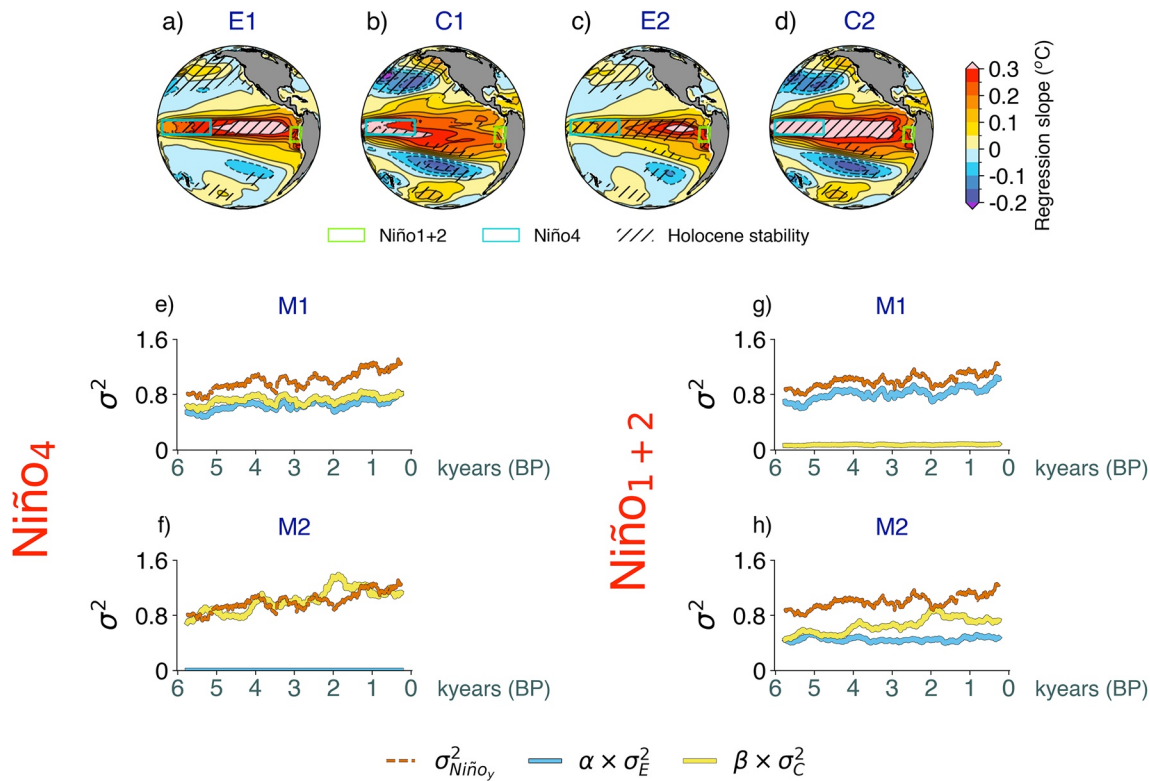


Figure 2. El Niño flavor patterns from 6,000 to 0 BP for (a), (b) M1 and (c), (d) M2 in the Sr02 simulation. The patterns are the regressed SST anomalies onto the E or C flavors. The blue and green boxes represent the Niño4 and Niño1+2 boxes, respectively. Solid (dashed) contours denote positive (negative) values. To estimate the significance of the pattern changes over the last 6,000 years, for each simulation and method, we performed a recomputation of the E and C regressed patterns every 50 years. We then calculated the standard deviation at each grid point for each set of 120 patterns we obtained after the recomputation. Hatches represent areas where the signal exceeds 1.2 times the average standard deviation. We call this criterion “Holocene stability,” representing areas with the most robust patterns over the last 6,000 years. For each method, we show the variance explained by the E and C flavors in the (e), (g) Niño1+2 and (f), (h) Niño4 boxes in the Sr02 simulation (see Methods section). The y-coordinate represents the variance. The red dotted lines are the 500-year rolling variance in the Niño boxes, and the blue and yellow solid lines are respectively the regressed 500-year rolling variance of the E and C flavors in the Niño boxes.

between the two periods and datasets can also be attributed to how ship observation biases were estimated before 1950. For ERSSTv5, the nighttime marine air temperature helps correct the ship observations' biases. 140 Empirical Orthogonal Teleconnections (EOT) were also used to reconstruct an SST field from 1854 to the present (Huang et al., 2018). For COBE-SST2, a bucket model calculates the biases of ship observations before 1941. 133 EOF modes were used to reconstruct monthly SSTs from 1850 to today (Huang et al., 2018). Our analysis shows that the estimates of M1 and M2 are sensitive to climatic changes between two short and close periods, and different observational products.

The methods could also be affected by the IPSL model not reproducing the correct ENSO flavors. If we focus on the Holocene, we find opposite slopes of the simulated variance ratios between M1 and M2. However, if we focus on shorter time scales, for example, the last three time periods in the simulations, they show how variable the variance ratio of E over C is for both methods (Figures 1a and 1b). For 1854–1950, the variance ratio of M2 in the simulations is compatible with ERSSTv5 but not COBE-SST2 (Figure 1c). The range of M1 and M2's variance ratios computed with COBE-SST2 seem to have stayed about the same between 1854–1950 and 1950–2019, contrary to ERSSTv5. Because of the sparse data before 1950, the methods used to reconstruct the SST field, and the biases, we cannot discuss the change in variability in detail. Also, we note the too-little length of observational windows to properly account for the chaotic nature of ENSO diversity. This model-data comparison indicates that despite the model biases and with the agreement regarding ERSSTv5 on the range of the variances of M1 and M2, we can use the simulations and discuss the evolution of the El Niño flavors during the Holocene. For the rest of this study, we focus on the Sr02 simulation since V1r01 and Sr02 have similar trends in the Holocene (Figures 1a and 1b).

3.2. Differences in ENSO Flavor Patterns

Another explanation for the difference in the variance ratio of E over C between the two periods of observations stems from the ENSO flavor patterns. In the observations, the patterns of E_1 and E_2 share similarities between 1950 and 2019 (Figure S2 in Supporting Information S1) and 1854–1950 (Figure S3 in Supporting Information S1), but there are some non-negligible differences. The C patterns are different in both present time frames, with C_2 extending to the Peruvian coast compared to C_1 . The E and C pattern differences between methods are also seen in the historical period of the simulations (Figures S2 and S3 in Supporting Information S1).

The simulated patterns for the Holocene also show similar differences (Figure 2). To understand the Holocene differences between M1 and M2, we focus on the evolution of each of the variances explained by each flavor in the eastern (Niño1+2) and the western (Niño4) ends of the Pacific. The pattern of E_1 is confined to the central-to-eastern part of the basin, while E_2 is only confined to the east. E_1 and E_2 show greater variance explained in the Niño1+2 box over the Holocene. E_2 explains almost no variance in the Niño4 box, compared with E_1 . Overall, M1 and M2 have similar shapes for the E flavor, but the amplitude is much larger in M1. For the C flavor, the differences in patterns are more drastic. C_2 spreads out over the whole basin compared to only the western part for C_1 (Figure 2). This results in C_2 having a variance explained in the Niño1+2 and Niño4 boxes, compared to only the Niño4 box for C_1 . Thus, ENSO flavor changes seem inconsistent between methods because they do not describe the same flavor patterns.

Inconsistency between methods could arise from M2, which is based on an approximation of M1 for the 1950–2010 period in Takahashi et al. (2011). We recomputed the coefficients in Equations 3 and 4 using E_1 and C_1 as references over the 6,000–0 BP interval. For Sr02, we have $E_2 = -0.32 \times Ni\tilde{n}o_4 + 2.28 \times Ni\tilde{n}o_{1+2}$ and $C_2 = 2.85 \times Ni\tilde{n}o_4 - 1.41 \times Ni\tilde{n}o_{1+2}$. We represent the variance ratio of the new E_2 and C_2 estimates (“M2 redone”) in Figure 3). The M1 and “M2 redone” variance ratios match better in the Holocene, but overall trends still differ. If we look at the period 6–5 kyr BP, the variance ratio of “M2 redone” says that the variance of E events is superior to C events; it is the opposite for M1. Figure 3 also shows variance ratios for the methods of Carré et al. (2021) and Ren and Jin (2011). Note that over the historical period Carré et al. (2021) capture the same fluctuations as the other indicators but with reduced magnitude (Figure S1 in Supporting Information S1). This can be attributed to the fact that the EP box chosen where data are available is only a proxy of the Niño1+2 box and located entirely south of the equator. The different ENSO metrics give different variance ratios over the Holocene, suggesting that calibration alone cannot solve the problem.

ENSO variability was weaker in the mid-Holocene compared to present-day as models and data suggest (Carré et al., 2021; Cobb et al., 2013; Emile-Geay et al., 2016). The mean state of the Pacific Ocean has changed under insolation forcing over the last 6,000 years; thus, we need to consider it. In the mid-Holocene, the thermocline feedback weakened, reducing ENSO variability. The weakening was linked to changes in the ocean currents. Specifically, enhanced surface poleward meridional currents reduced the Bjerknes feedback, that is, the response of anomalous thermocline depth to the zonal wind stress anomaly (An & Choi, 2014; Chen et al., 2019; Iwakiri &

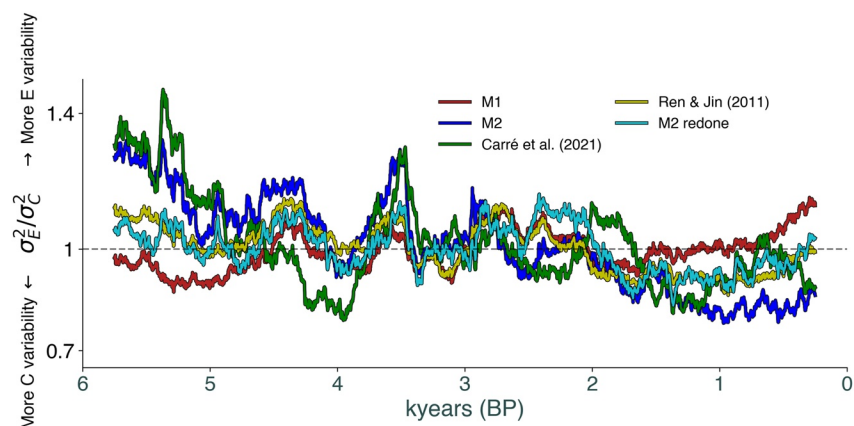


Figure 3. Variances ratios of E over C during the Holocene for the Sr02 simulation. The variance ratios were computed using 500-year moving windows spanning from 6,000 to 0 BP. See Supporting Information S1 for the definitions of Ren and Jin (2011) and Carré et al. (2021). Above the $y = 1$ dashed line, the variance of the E flavor is greater than the C flavor, and the inverse for below. Same figure is shown in the additional material, for the Vlr01 simulation (Figure S5 in Supporting Information S1).

Watanabe, 2019). Also, the tropical Pacific's thermocline was more diffuse and less stratified than in the present due to a more pronounced zonal tilt (Figure S4a in Supporting Information S1) and colder surface temperatures (Figure S4b in Supporting Information S1). On average, ENSO activity was more confined and attached to a less developed equatorial upwelling structure in the mid-Holocene (An et al., 2018; Braconnot et al., 2012; Iwakiri & Watanabe, 2019; Luan et al., 2012). With time, ENSO activity strengthened and could develop more over the tropical basin (An et al., 2018; Iwakiri & Watanabe, 2019). If we go back to the patterns of C_2 and E_1 , they have their center of action over most of the Pacific (Figure 3). Therefore, the increase in variance of C_2 and E_1 over both Niño boxes should be interpreted as an increase in El Niño activity extending east and west.

4. Discussion and Conclusions

In this paper, we chose two methods of computing E and C flavors in the tropical Pacific Ocean, following Takahashi et al. (2011)'s study, and looked at their changes over 6,000 years with transient simulations. In instrumental data, we show that the two methods are almost the same in the present (1950–2019), but discrepancies arise when looking at an adjacent period (1854–1950). In the simulations, on even longer time scales, we find opposite results between M1 and M2. The concepts of E and C flavors do not translate the same for M1 and M2. In the simulations, the C_2 pattern dominates the tropical Pacific and exhibits a higher weight in terms of explained variance than the E_2 pattern. In contrast, the simulated E_1 pattern forms in the central-to-east part of the basin, while the simulated C_1 pattern is confined to the western side. Although seemingly contradictory over the last 6,000 years, both methods conclude for their dominant flavor (E for M1 and C for M2) that their variance signal has spread to the east and western part of the tropical Pacific Ocean, thus expressing a westward and eastward expansion of El Niño variance. This is dynamically in accordance with the thermocline feedback changes that occurred during the Holocene. The opposite results between M1 and M2 could lead to opposite conclusions without proper interpretation, even if calibration is considered. The indicators used in this study, and most El Niño indicators in general, are designed with frameworks that are too restricted.

To study past changes in El Niño flavors, one would assume that M2 is the best choice since it uses regional boxes in its definition, allowing for better comparison to data. Carré et al. (2021) used the ERSSTv5 dataset from 1900 to 2017 to compare the variance ratio of their defined EP and CP boxes with the variance ratio of E_2 and C_2 . They matched, albeit with minor differences in magnitude. However, two boxes do not suffice to cover the E and C flavor pattern shifts over time. We could consider M1 to be the most rigorous method due to its ability to properly distinguish unique pattern characteristics between E and C flavors. However, comparing the results from M1 to the boxes defined by the paleo-archives' location is not viable, since these boxes fail to encompass the two patterns resulting from the EOF rotation.

Our results imply that different techniques of detecting E or C flavor-like El Niño events in models and observations could lead to incoherent results. A suggestion for using M2 would be to make sure that the linear regression coefficients (Equations 3 and 4) are computed for the study's time frame (in models or observations) instead of taking them directly from Takahashi et al. (2011). This is true for other methods that use the linear combination of Niño or regional boxes.

It is important to note that these findings do not imply the superiority of one method over the other. Furthermore, we strongly advise caution in future studies that employ techniques to differentiate El Niño flavors based on present conditions, as variations in the mean state can introduce discrepancies between methods that are expected to estimate similar ENSO variances. This is already the case with the results from the last IPCC report regarding El Niño flavor changes in the future. In models that have an El Niño-like warming, Fredriksen et al. (2020) estimate an increase in EP ENSO events while Freund et al. (2020) predict more CP and fewer EP events. Our results indicate that their contradictory conclusions stem from the difference in the methods used to characterize ENSO flavors. The apparent differences in results will cause a misinterpretation that could affect how they will be used to characterize future changes in ENSO characteristics.

Data Availability Statement

The processed data are available at <https://doi.org/10.6084/m9.figshare.20789203> and the Jupyter Notebook used to make the figures is available at <https://github.com/iadicarlo/elniño-flavors-paper> (<https://doi.org/10.5281/zenodo.7938040>). We acknowledge NOAA/OAR/ESRL PSL, USA for providing us the COBE-SST2 and ERSSTv5 data respectively at <https://psl.noaa.gov/data/gridded/data.cobe2.html> and <https://psl.noaa.gov/data/gridded/data.noaa.ersst.v5.html>.

Acknowledgments

This study is part of the CNRS LEFE-IMAGO MOSCA project. The simulations were performed using HPC resources from GENCI-TGCC (gen2212, gen12006). Isma Abdelkader Di Carlo is funded through a doctoral contract from ENS Paris.

References

An, S.-I., & Choi, J. (2014). Mid-Holocene tropical Pacific climate state, annual cycle, and ENSO in PMIP2 and PMIP3. *Climate Dynamics*, 43(3), 957–970. <https://doi.org/10.1007/s00382-013-1880-z>

An, S.-I., Im, S.-H., & Jun, S.-Y. (2018). Changes in ENSO activity during the last 6,000 years modulated by background climate state. *Geophysical Research Letters*, 45(5), 2467–2475. <https://doi.org/10.1002/2017GL076250>

Ashok, K., Behera, S. K., Rao, S. A., Weng, H., & Yamagata, T. (2007). El Niño Modoki and its possible teleconnection. *Journal of Geophysical Research*, 112(C11), C11007. <https://doi.org/10.1029/2006JC003798>

Bellenger, H., Guilyardi, E., Leloup, J., Lengaigne, M., & Vialard, J. (2014). Enso representation in climate models: From CMIP3 to CMIP5. *Climate Dynamics*, 42(7), 1999–2018. <https://doi.org/10.1007/s00382-013-1783-z>

Braconnot, P., Luan, Y., Brewer, S., & Zheng, W. (2012). Impact of Earth’s orbit and freshwater fluxes on Holocene climate mean seasonal cycle and ENSO characteristics. *Climate Dynamics*, 38(5), 1081–1092. <https://doi.org/10.1007/s00382-011-1029-x>

Braconnot, P., Zhu, D., Marti, O., & Servonnat, J. (2019). Strengths and challenges for transient mid- to late Holocene simulations with dynamical vegetation. *Climate of the Past*, 15(3), 997–1024. <https://doi.org/10.5194/cp-15-997-2019>

Brown, J. R., Brierley, C. M., An, S.-I., Guarino, M.-V., Stevenson, S., Williams, C. J. R., et al. (2020). Comparison of past and future simulations of ENSO in CMIP5/PMIP3 and CMIP6/PMIP4 models. *Climate of the Past*, 16(5), 1777–1805. <https://doi.org/10.5194/cp-16-1777-2020>

Cai, W., Borlace, S., Lengaigne, M., van Rensch, P., Collins, M., Vecchi, G., et al. (2014). Increasing frequency of extreme El Niño events due to greenhouse warming. *Nature Climate Change*, 4(2), 111–116. <https://doi.org/10.1038/nclimate2100>

Cai, W., Santoso, A., Collins, M., Dewitte, B., Karamperidou, C., Kug, J.-S., et al. (2021). Changing El Niño–Southern Oscillation in a warming climate. *Nature Reviews Earth & Environment*, 2(9), 628–644. <https://doi.org/10.1038/s43017-021-00199-z>

Callahan, C. W., Chen, C., Rugenstein, M., Bloch-Johnson, J., Yang, S., & Moyer, E. J. (2021). Robust decrease in El Niño/Southern Oscillation amplitude under long-term warming. *Nature Climate Change*, 11(9), 752–757. <https://doi.org/10.1038/s41558-021-01099-2>

Capotondi, A., Wittenberg, A. T., Newman, M., Lorenzo, E. D., Yu, J.-Y., Braconnot, P., et al. (2015). Understanding ENSO diversity. *Bulletin of the American Meteorological Society*, 96(6), 921–938. <https://doi.org/10.1175/BAMS-D-13-00117.1>

Carré, M., Braconnot, P., Elliot, M., d’Agostino, R., Schurer, A., Shi, X., et al. (2021). High-resolution marine data and transient simulations support orbital forcing of ENSO amplitude since the mid-Holocene. *Quaternary Science Reviews*, 268, 107125. <https://doi.org/10.1016/j.quascirev.2021.107125>

Carré, M., Sachs, J. P., Purca, S., Schauer, A. J., Braconnot, P., Falcón, R. A., et al. (2014). Holocene history of ENSO variance and asymmetry in the eastern tropical Pacific. *Science*, 345(6200), 1045–1048. <https://doi.org/10.1126/science.1252220>

Chen, L., Zheng, W., & Braconnot, P. (2019). Towards understanding the suppressed ENSO activity during mid-Holocene in PMIP2 and PMIP3 simulations. *Climate Dynamics*, 53(1), 1095–1110. <https://doi.org/10.1007/s00382-019-04637-z>

Cobb, K. M., Westphal, N., Sayani, H. R., Watson, J. T., Di Lorenzo, E., Cheng, H., et al. (2013). Highly variable El Niño–Southern oscillation throughout the Holocene. *Science*, 339(6115), 67–70. <https://doi.org/10.1126/science.1228246>

Collins, M., An, S.-I., Cai, W., Ganachaud, A., Guilyardi, E., Jin, F.-F., et al. (2010). The impact of global warming on the tropical Pacific Ocean and El Niño. *Nature Geoscience*, 3(6), 391–397. <https://doi.org/10.1038/ngeo0868>

DiNezio, P. N., Kirtman, B. P., Clement, A. C., Lee, S.-K., Vecchi, G. A., & Wittenberg, A. (2012). Mean climate controls on the simulated response of ENSO to increasing greenhouse gases. *Journal of Climate*, 25(21), 7399–7420. <https://doi.org/10.1175/JCLI-D-11-00494.1>

Dufresne, J.-L., Foujols, M.-A., Denvil, S., Caubel, A., Marti, O., Aumont, O., et al. (2013). Climate change projections using the IPSL-CM5 Earth System model: From CMIP3 to CMIP5. *Climate Dynamics*, 40(9), 2123–2165. <https://doi.org/10.1007/s00382-012-1636-1>

Emile-Geay, J., Cobb, K., Carré, M., Braconnot, P., Leloup, J., Zhou, Y., et al. (2016). Links between tropical Pacific seasonal, interannual and orbital variability during the Holocene. *Nature Geoscience*, 9(2), 168–173. <https://doi.org/10.1038/ngeo2608>

Fredriksen, H.-B., Berner, J., Subramanian, A. C., & Capotondi, A. (2020). How does El Niño–Southern Oscillation change under global warming—A first look at CMIP6. *Geophysical Research Letters*, 47(22), e2020GL090640. <https://doi.org/10.1029/2020GL090640>

Freund, M. B., Brown, J. R., Henley, B. J., Karoly, D. J., & Brown, J. N. (2020). Warming patterns affect El Niño diversity in CMIP5 and CMIP6 models. *Journal of Climate*, 33(19), 8237–8260. <https://doi.org/10.1175/JCLI-D-19-0890.1>

Hirahara, S., Ishii, M., & Fukuda, Y. (2014). Centennial-scale sea surface temperature analysis and its uncertainty. *Journal of Climate*, 27(1), 57–75. <https://doi.org/10.1175/JCLI-D-12-00837.1>

Huang, B., Angel, W., Boyer, T., Cheng, L., Chepurin, G., Freeman, E., et al. (2018). Evaluating SST analyses with independent ocean profile observations. *Journal of Climate*, 31(13), 5015–5030. <https://doi.org/10.1175/jcli-d-17-0824.1>

Huang, B., Thorne, P. W., Banzon, V. F., Boyer, T., Chepurin, G., Lawrimore, J. H., et al. (2017). Extended reconstructed sea surface temperature, version 5 (ERSSTv5): Upgrades, validations, and intercomparisons. *Journal of Climate*, 30(20), 8179–8205. <https://doi.org/10.1175/JCLI-D-16-0836.1>

Iwakiri, T., & Watanabe, M. (2019). MECHANISMS Reducing ENSO amplitude and asymmetry via an enhanced seasonal cycle in the mid-Holocene. *Journal of Climate*, 32(23), 8069–8085. <https://doi.org/10.1175/JCLI-D-19-0110.1>

Kao, H.-Y., & Yu, J.-Y. (2009). Contrasting eastern-Pacific and central-Pacific types of ENSO. *Journal of Climate*, 22(3), 615–632. <https://doi.org/10.1175/2008JCLI2309.1>

Karamperidou, C., Di Nezio, P. N., Timmermann, A., Jin, F.-F., & Cobb, K. M. (2015). The response of ENSO flavors to mid-Holocene climate: Implications for proxy interpretation. *Paleoceanography*, 30(5), 527–547. <https://doi.org/10.1002/2014PA002742>

Kug, J.-S., Jin, F.-F., & An, S.-I. (2009). Two types of El Niño events: Cold tongue El Niño and warm pool El Niño. *Journal of Climate*, 22(6), 1499–1515. <https://doi.org/10.1175/2008JCLI2624.1>

Lee, T., & McPhaden, M. J. (2010). Increasing intensity of El Niño in the central-equatorial Pacific. *Geophysical Research Letters*, 37(14), L14603. <https://doi.org/10.1029/2010GL044007>

Luan, Y., Braconnot, P., Yu, Y., Zheng, W., & Marti, O. (2012). Early and mid-Holocene climate in the tropical Pacific: Seasonal cycle and inter-annual variability induced by insolation changes. *Climate of the Past*, 8(3), 1093–1108. <https://doi.org/10.5194/cp-8-1093-2012>

McPhaden, M. J., Lee, T., & McClurg, D. (2011). El Niño and its relationship to changing background conditions in the tropical Pacific Ocean. *Geophysical Research Letters*, 38(15), L15709. <https://doi.org/10.1029/2011GL048275>

Otto-Bliessner, B. L., Braconnot, P., Harrison, S. P., Lunt, D. J., Abe-Ouchi, A., Albani, S., et al. (2017). The PMIP4 contribution to CMIP6 – Part 2: Two interglacials, scientific objective and experimental design for Holocene and Last Interglacial simulations. *Geoscientific Model Development*, 10(11), 3979–4003. <https://doi.org/10.5194/gmd-10-3979-2017>

Philander, S. G. (1990). *El Niño, La Niña, and the Southern Oscillation* (Vol. 46). Academic Press.

Ren, H.-L., & Jin, F.-F. (2011). Niño indices for two types of ENSO. *Geophysical Research Letters*, 38(4), L04704. <https://doi.org/10.1029/2010GL046031>

- Saint-Lu, M., Braconnot, P., Leloup, J., & Marti, O. (2016). The role of El Niño in the global energy redistribution: A case study in the mid-Holocene. *Climate Dynamics*, 52(12), 7135–7152. <https://doi.org/10.1007/s00382-016-3266-5>
- Stevenson, S., McGregor, H. V., Phipps, S. J., & Fox-Kemper, B. (2013). Quantifying errors in coral-based ENSO estimates: Toward improved forward modeling of $\delta^{18}\text{O}$. *Paleoceanography*, 28(4), 633–649. <https://doi.org/10.1002/palo.20059>
- Takahashi, K., Montecinos, A., Goubanova, K., & Dewitte, B. (2011). ENSO regimes: Reinterpreting the canonical and Modoki El Niño. *Geophysical Research Letters*, 38(10), L10704. <https://doi.org/10.1029/2011GL047364>
- Tibshirani, R. (1996). Regression Shrinkage and Selection via the Lasso. *Journal of the Royal Statistical Society: Series B*, 58(1), 267–288. <https://doi.org/10.1111/j.2517-6161.1996.tb02080.x>
- Timmermann, A., An, S.-I., Kug, J.-S., Jin, F.-F., Cai, W., Capotondi, A., et al. (2018). El Niño–Southern Oscillation complexity. *Nature*, 559(7715), 535–545. <https://doi.org/10.1038/s41586-018-0252-6>
- Vecchi, G. A., & Wittenberg, A. T. (2010). El Niño and our future climate: Where do we stand? *Wiley Interdisciplinary Reviews: Climate Change*, 1(2), 260–270. <https://doi.org/10.1002/wcc.33>
- Wengel, C., Lee, S.-S., Stuecker, M. F., Timmermann, A., Chu, J.-E., & Schloesser, F. (2021). Future high-resolution El Niño/Southern Oscillation dynamics. *Nature Climate Change*, 11(9), 758–765. <https://doi.org/10.1038/s41558-021-01132-4>
- Wittenberg, A. T. (2009). Are historical records sufficient to constrain ENSO simulations? *Geophysical Research Letters*, 36(12), L12702. <https://doi.org/10.1029/2009GL038710>
- Yeh, S.-W., Kug, J.-S., Dewitte, B., Kwon, M.-H., Kirtman, B. P., & Jin, F.-F. (2009). El Niño in a changing climate. *Nature*, 461(7263), 511–514. <https://doi.org/10.1038/nature08316>